Spiral-shaped scattered field from incident evanescent acoustic waves on a Mie Particle

Journal of Physics: Conference Series **1761** (2021) 012003 doi:10.1088/1742-6596/1761/1/012003

Spiral-shaped scattered field from incident evanescent acoustic waves on a Mie Particle

Ludovic Alhaïtz, Diego Baresch, Thomas Brunet, Christophe Aristégui, Olivier Poncelet

Univ. Bordeaux, CNRS, Bordeaux INP, ENSAM, INRAE, UMR 5295 I2M, F-33405 Talence, France

E-mail: ludovic.alhaitz@u-bordeaux.fr

Abstract. We consider theoretically the scattering of an incident evanescent plane wave by a spherical particle. The scattering problem is treated in a classic way by applying the T-matrix formalism and the resulting field is expressed on the basis of the different vibration modes of the particle. Compared to the case of a homogeneous plane incident wave, additional azimuthal scattered modes are excited and their contribution provokes a symmetry breaking of the field. Importantly, if a mode is preferentially excited by choosing the corresponding reduced frequency, the scattered radiation exhibits a spiral structure. The scattered field has a rotating phase around the scatterer which comes from the formation of spiral scattered waves and this effect is accentuated by increasing the evanescence degree of the incident wave. These results could have important implications for the contactless manipulation of objects with acoustic radiation forces and torques.

1. Introduction

Evanescent waves are inhomogeneous waves naturally occurring near the surface of objects and their interaction with particles may lead to several functional applications. For exemple they are used in optics or acoustics for sub-wavelength imaging which consists in investigating the near field of objects using a probe to collect the evanescent components of the field spatially richer than those of homogeneous waves [1]. They are also exploited for microfluidics devices [2] or for the search of sediments in the naval sector [3]. Moreover, an important experiment demonstrated the possibility to move particles in an evanescent optical field thanks to the radiation force induced [4]. Recently, interest has increased in characterizing their non-classical properties [5], particularly because of potential applications for particle trapping using laser light or ultrasonic beams [6, 7].

The scattering problem was investigated few decades ago for optical waves and it has been shown that additional mode contributions can be strongly enhanced in the scattering of an evanescent wave compared to a homogeneous wave [8, 9]. An efficient method was proposed recently for the calculation of Mie scattering solutions for an incident evanescent wave by considering matrix rotations around a complex-valued angle [10]. The present article focus on the intriguing structure of the field resulting from the scattering. Semi-analytical expressions are derived for the scattering of an incident evanescent harmonic wave and a modal field analysis is proposed to understand the interaction with a Mie particle. This work could be helpful to

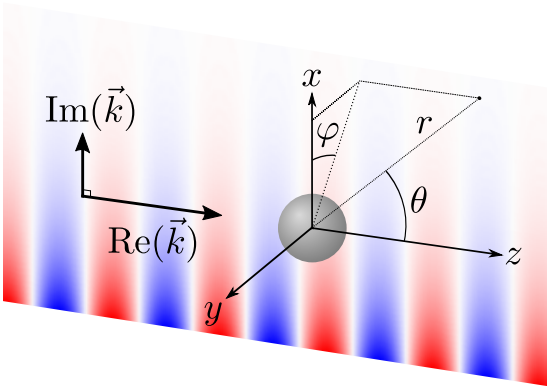

Figure 1: Scattering problem configuration of an incident evanescent plane wave on a sphere, propagating along the z-axis and decaying along the x-axis. The real part and imaginary part of the complex wave vector $\vec{k}$ are mutually orthogonal. The centers of the coordinates systems coincide with the center of the sphere, θ and φ are respectively the polar and the azimuthal angles.

understand the propagation of surface waves in heterogeneous media as in seismology or non destructive testing, but also for applications in acoustic imaging or particle manipulation.

2. The scattering problem

A theoretical framework is developed to model the scattering of an incident evanescent plane wave propagating in an inviscid medium by a spherical resonant particle (Mie regime) made of an inviscid fluid also. We assume that the incident field extends to infinity in order to analyze the interaction between the incident wave and the particle only. We do not matter how this evanescent wave is generated or if it is close to a surface.

The spatial part of the complex-valued acoustic field is expressed from the acoustic velocity-potential $\phi(r,\theta,\varphi)$ and is time-harmonic dependent with the $\mathrm{e}^{-\mathrm{i}\omega t}$ convention. Velocity and pressure fields are given by $\vec{v}(r,\theta,\varphi) = \overrightarrow{\nabla}\phi(r,\theta,\varphi)$ and $p(r,\theta,\varphi) = \rho_0 \mathrm{i}\omega\phi(r,\theta,\varphi)$, where ρ_0 is the mass density of the surrounding medium and ω the pulsation. The potential ϕ satisfies the Helmholtz equation $(\Delta + k_0^2)\,\phi = 0$ where $k_0 = \omega/c_0$ is the real-valued wavenumber in the surrounding medium of sound speed c_0. The same set of equations applies for the field inside the spherical scatterer by replacing ρ_0 by ρ_1, k_0 by k_1, and c_0 by c_1.

2.1. Modal field expressions and T-matrix

The incident velocity-potential solution of the propagation equation is generally expanded in the spherical harmonics basis in terms of partial mode series as:

$$\phi_{\mathrm{i}}(r,\theta,\varphi) = \sum_{n=0}^{+\infty}\sum_{m=-n}^{n} a_n^m j_n(k_0 r) Y_n^m(\theta,\varphi) \tag{1}$$

where a_n^m are the shape coefficients, j_n are the spherical Bessel functions and $Y_n^m(\theta,\varphi) = \sqrt{\frac{2n+1}{4\pi}\frac{(n-m)!}{(n+m)!}} P_n^m(\cos\theta)\mathrm{e}^{\mathrm{i}m\varphi}$ are the orthonormal complex-valued spherical harmonics with P_n^m the associated Legendre functions.

The scattered field by the particle is expressed in terms of divergent spherical radial functions

as:

$$\phi_{\mathrm{s}}(r,\theta,\varphi) = \sum_{n=0}^{+\infty} \sum_{m=-n}^{n} s_n^m h_n^{(1)}(k_0 r) Y_n^m(\theta,\varphi) \tag{2}$$

were s_n^m are modal amplitudes and $h_n^{(1)}$ are the spherical Hankel functions of the first kind which are chosen to satisfy the Sommerfield radiation condition according to the temporal convention adopted. The modal amplitudes s_n^m are obtained by applying the T-matrix approach [14] and are proportional to shape coefficients of the incident field in our case:

$$s_n^m = S_n a_n^m \tag{3}$$

where S_n are the scattering coefficients independent of m (see (A.1)). These coefficients S_n are obtained by applying the continuity conditions of normal stress and normal displacement at the interface between the surrounding medium and the scatterer. Importantly, they are by definition independent from the shape of the incident field. This implies that for any type of incident wave, shape resonances in the scattered modal amplitudes appear at the same frequencies as for a homogeneous incident plane wave.

The scattering method is general for any incident wave and the following sections focus on the evanescent wave and its expression in the spherical basis.

2.2. Incident evanescent wave

We consider an evanescent incident plane harmonic wave which is propagating in an inviscid fluid medium along the z-direction with an exponential decrease in amplitude in the x-direction. The centers of the coordinates systems coincide with the center of the sphere, θ is the polar angle and φ is the azimuthal angle (see Fig. 1). The incident wave is thus definined by a complex-valued wave vector such that $\vec{k} = k_z \vec{e}_z + \mathrm{i}\kappa \vec{e}_x$ where k_z and κ are respectively the real wave number of propagation and the decay rate in amplitude in the orthogonal direction. Importantly, the fluid particle motion has an elliptical trajectory, since the polarization vector is a complex-valued vector proportional to the complex wave vector. The incident evanescent velocity-potential, which is symmetrical about the (xz)-plane, is then given by:

$$\phi_{\mathrm{i}}(x,z) = \phi_0 \, \mathrm{e}^{\mathrm{i}\vec{k}\cdot\vec{r}} = \phi_0 \, \mathrm{e}^{\mathrm{i}k_z z - \kappa x}. \tag{4}$$

ϕ_0 is the incident potential magnitude at $x = 0$ which implies that the field has an increasing magnitude for $x < 0$. Nevertheless, for our analysis the important parameter is the amplitude gradient effect. The dispersion relation of evanescent plane waves in a non-viscous fluid medium reads $\vec{k} \cdot \vec{k} = k_z^2 - \kappa^2 = k_0^2$. In order to compare the scattering of evanescent and homogeneous incident waves, we introduce the evanescence degree of the incident field $\beta = \kappa / k_z$. Therefore, the incident velocity-potential can be also written as $\phi_{\mathrm{i}}(x,z) = \phi_0 \, \mathrm{e}^{\mathrm{i}k_z(z+\mathrm{i}\beta x)}$. When $\beta = 0$, it corresponds to a homogenous incident wave, and $\beta \in]0,1[$ corresponds to an evanescent incident wave with an increasing decay rate with increasing values of β. Note that $\beta = 1$ is a limiting (non admissible) value. The decay rate in amplitude in the orthogonal direction as a function of β is $\kappa = \frac{\beta k_0}{\sqrt{1-\beta^2}} < k_z$.

2.3. Calculation of the shape coefficients for an evanescent plane wave

This kind of field is asymmetrical about the z-axis so azimuthal modes $m \neq 0$ must be taken into account in the modal expansion. To express the incident evanescent field in the form of (1), shape coefficients a_n^m can be obtained by projecting the exponential field (4) onto the spherical

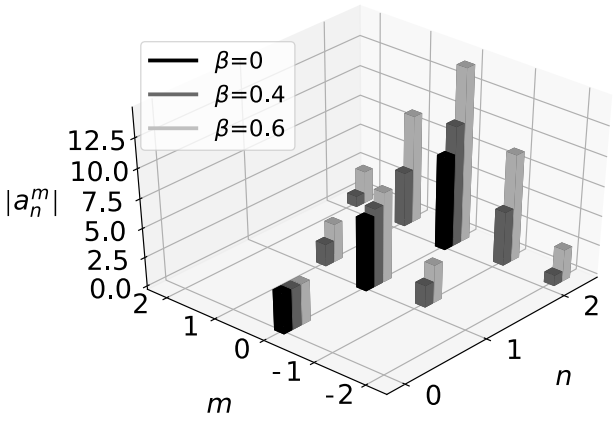

Figure 2: (n, m)-spectrum of the shape coefficients a_n^m of the incident field. For display reasons, sticks corresponding to $\beta > 0$ are slightly shifted along the n-axis.

harmonics using the orthogonality properties of this basis [11, 12, 13]. It leads to an integration over the solid angle Ω at a given radius $r = R$:

$$a_n^m = \frac{1}{j_n(k_0 R)} \int_\Omega \phi_\mathrm{i}(R, \theta, \varphi)\, \overline{Y_n^m(\theta, \varphi)}\, \mathrm{d}\Omega = \frac{\phi_0}{j_n(k_0 R)} \int_\Omega \mathrm{e}^{\mathrm{i}k_z R \cos\theta} \mathrm{e}^{-\kappa R \sin\theta \cos\varphi}\, \overline{Y_n^m(\theta, \varphi)}\, \mathrm{d}\Omega \quad (5)$$

where $\mathrm{d}\Omega = \sin\theta\, \mathrm{d}\theta \mathrm{d}\varphi$ and $\overline{Y_n^m}$ is the complex conjugate of spherical harmonics. The integration over the azimuthal angle φ is performed by identification:

$$\int_0^{2\pi} \mathrm{e}^{-\kappa R \sin\theta \cos\varphi} \mathrm{e}^{-\mathrm{i}m\varphi} \mathrm{d}\varphi = (-1)^m\ 2\pi I_m(\kappa R \sin\theta) \quad (6)$$

where I_m are the modified Bessel functions of the first kind. Finally, we obtain:

$$a_n^m = \phi_0\, \frac{(-1)^m}{j_n(k_0 R)} \sqrt{(2n+1)\pi \frac{(n-m)!}{(n+m)!}} \int_0^\pi \mathrm{e}^{\mathrm{i}k_z R \cos\theta} I_m(\kappa R \sin\theta) P_n^m(\cos\theta) \sin\theta \mathrm{d}\theta. \quad (7)$$

This provides a method to comptute the a_n^m coefficients semi-analytically by a single numerical integration over the polar angle θ. We verified that they are frequency independent as long as the radius R is carefully chosen so that the product $k_0 R$ does not correspond to a zero of the j_n functions. One can note that $a_n^{-m} = (-1)^m a_n^m$.

The moduli of shape coefficients are plotted in Fig. 2 and show that for an evanescent wave, the energy is distributed over more harmonics than for a homogeneous wave. The amplitude of these additional modes $a_n^{m\neq 0}$ strongly depends on the value of the evanescence degree β. By increasing β, the incident field has a higher amplitude gradient and therefore the scattered field will be more and more asymmetrical about the z-axis.

2.4. Scattered field

As $Y_n^{-m} = (-1)^m\, \overline{Y_n^m}$ and by taking into account modal symmetries $s_n^{-m} = (-1)^m\, s_n^m$ following (3), the scattered field expression (2) in the case of an evanescent incident wave can be written

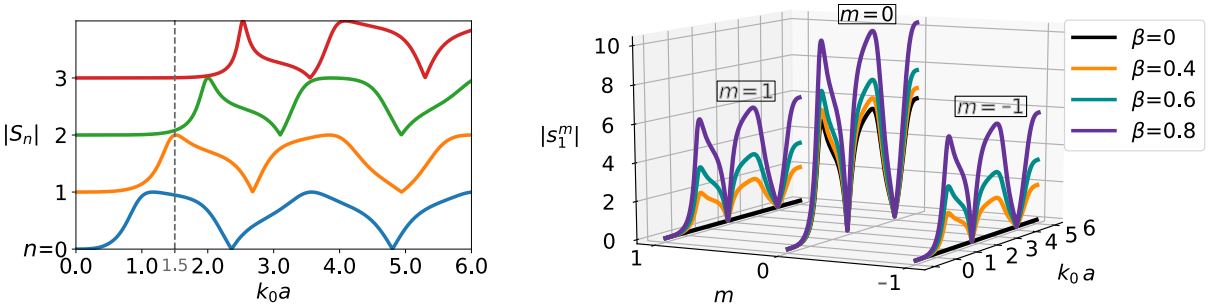

(a) (b)

Figure 3: (a) Moduli of scattering coefficients S_n as a function of the reduced frequency k_0a. The surrounding medium is water ($\rho_0 = 1000$ kg/m^3, $c_0 = 1485$ m/s) and the scatterer is a FC40 oil droplet ($\rho_1 = 1850$ kg/m^3, $c_1 = 640$ m/s). (b) Moduli of modal amplitudes s_n^m of the scattered field for the dipolar mode $n = 1$ and different evanescent degrees β of the incident field.

as follows:

$$\begin{aligned}\phi_{\mathrm{s}}(r,\theta,\varphi) &= \sum_{n=0}^{+\infty}\sum_{m=0}^{n} s_n^m h_n^{(1)}(k_0 r)\left[Y_n^m(\theta,\varphi) + \overline{Y_n^m(\theta,\varphi)}\right]\left(1-\frac{\delta_{m0}}{2}\right)\\ &= \sum_{n=0}^{+\infty}\sum_{m=0}^{n} s_n^m h_n^{(1)}(k_0 r)\tilde{P}_n^m(\cos\theta)\cos(m\varphi)(2-\delta_{m0}) \end{aligned} \tag{8}$$

where $\tilde{P}_n^m(\cos\theta) = \sqrt{\frac{2n+1}{4\pi}\frac{(n-m)!}{(n+m)!}}P_n^m(\cos\theta)$ and δ is the Kronecker symbol. As the incident field, the scattered field is symmetrical in φ. The field can be angularly constant about the azimuthal angle φ or not depending on whether the incident wave is homogeneous or evanescent. The field symmetry about the horizontal (yz)-plane can be altered and the purpose of the following section is to analyse the differencies on both sides of this plane.

3. Spiral-shaped scattered field and resonances

The scattering by a spherical fluid particle is analysed in this section. The scatterer is chosen to be a non-viscous spherical FC40 oil droplet which exhibits clear Mie resonances [15, 16]. Therefore, the amplitude of the scattered field by such a scatterer is enhanced in the total field.

3.1. Dipolar resonance

We firstly analyse the dipolar behavior of the scatterer. We hence choose the reduced frequency corresponding to the dipolar resonnance of the particle ($n = 1$, $k_0a = 1.5$). For this frequency, the scattering coefficient S_1 of the dipolar mode is predominant in comparison with other higher vibration modes (see Fig. 3a).

The moduli of scattered modal amplitudes for the dipolar mode $n = 1$ are plotted in Fig. 3b. Interestingly, the modal richness of the evanescent incident wave provides an enhanced scattered modal content. Indeed, all azimuthal scattered modes $m \neq 0$ are null for a homogenous incident wave ($\beta = 0$) because the field has no azimuthal dependence by symmetry. For an evanescent incident wave with $\beta \neq 0$, azimuthal scattered modes are excited and their amplitude can be tuned by varying β. This characteristic could be exploited, for exemple, for acoustic field shaping applications.

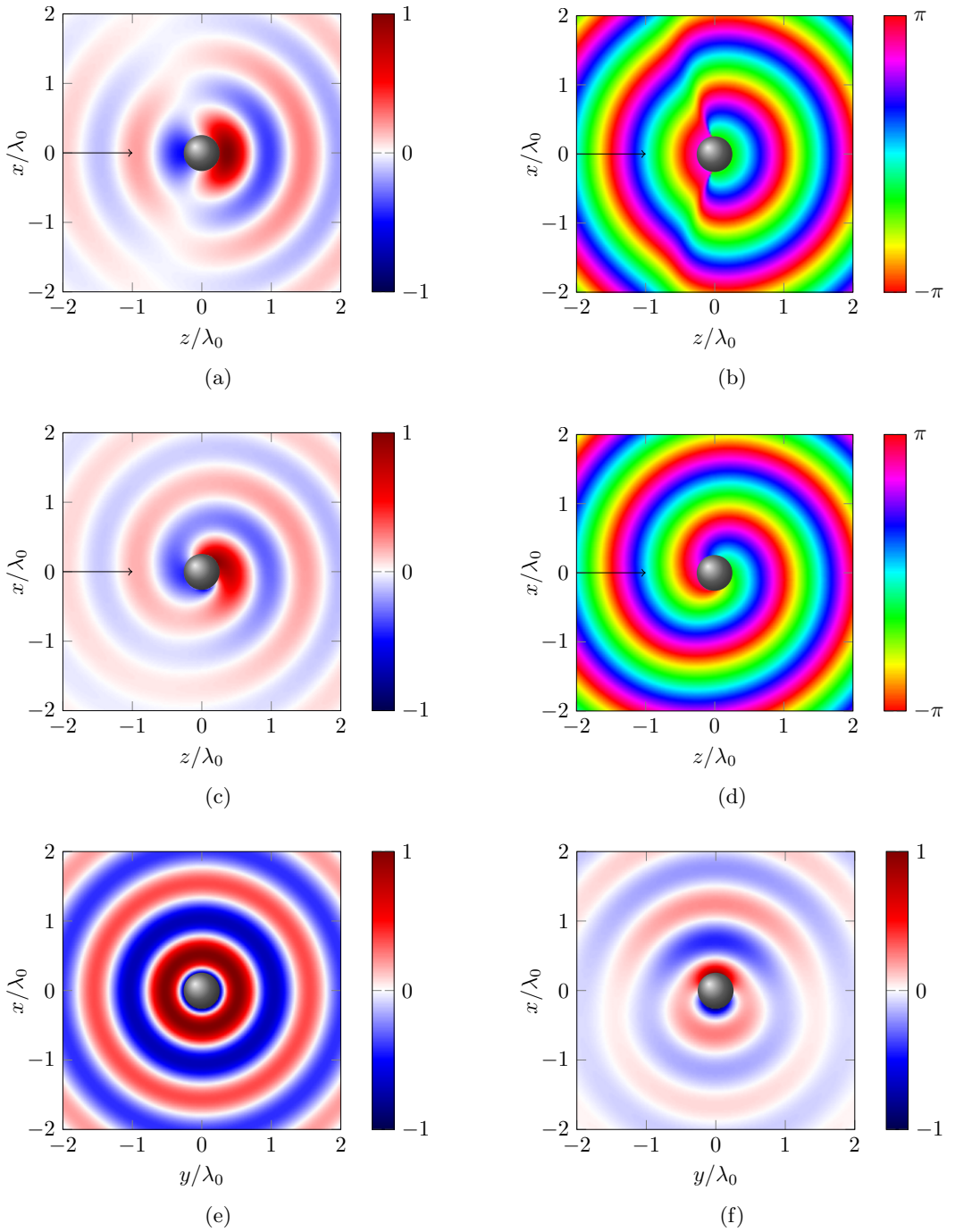

Figure 4: Figures a-d show the real part and phase of the scattered acoustic pressure field in the (xz)-plane for the reduced frequency $k_0a = 1.5$ corresponding to the dipolar resonance. This field is calculated for a homogeneous incident wave (a, b) and for an evanescent wave with $\beta = 0.6$ (c, d). Figures e, f show the real part of the scattered pressure field in the transversal (xy)-plane for a homogeneous (e) and an evanescent incident wave with $\beta = 0.6$ (f) at the same reduced frequency. All amplitudes are normalized by the maximum of pressure and the black arrow shows the propagation direction of the incident wave.

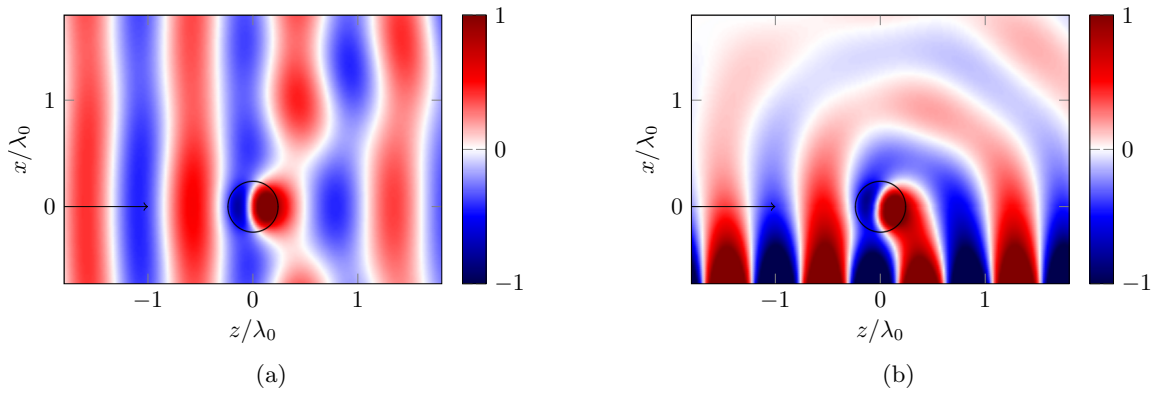

Figure 5: Real part of the total acoustic pressure field and the pressure field inside the particle in the (xz)-plane for a homogeneous (a) and an evanescent incident wave with $\beta = 0.4$ (b) at $k_0 a = 1.5$.

The scattered pressure field is computed comparatively for a homogeneous and an evanescent incident wave. For a given frequency $f = 300$ kHz, the particle radius is chosen to excite the dipolar resonance $k_0 a = 1.5$. The real part and phase of the scattered field are shown in Fig. 4 for different display planes. If the incident wave is homogeneous, the scattered field is symmetrical about the z-direction and we can see a strong dipolar contribution in this direction coupled with the monopolar one. Remarkably, if the incident wave is evanescent with a sufficient evanescence degree β, the wavefront of the scattered field has a spiral-like shape around the scatterer. In the transversal (xy)-plane, the radiation of the sphere is isotropic for a homogeneous incident wave, whereas it has a dipole-like structure for the evanescent case. Due to the amplitude gradient in the incident field, the sphere is allowed to oscillate in the x-direction and the radiation is amplified in the direction of the exponential decay (*i.e.* for $x > 0$). In summary, the field symmetry is broken in the evanescent configuration which can lead to a spiral effect in the scattered field.

The acoustic field shown in Fig. 5 corresponds to the field inside the scatterer, and to the total field in the surrounding medium which is the superposition of the incident field and the scattered field. On the Fig. 5a, the incident wave is homogeneous and most of the scattered energy is directed in the z-direction. On the other hand, for an incident evanescent wave the scattered field dominates the incident field where the latter has a low amplitude, typically above the particle in the (xz)-plane. In this region, the field is circular and propagates in all directions (see Fig. 5b).

3.2. Spiral waves in details

In order to understand the spiral effect observations presented in the last section, we derive analytical expressions of the scattered field which include spiral waves, *i.e.* waves which have an angular phase propagation.

Since the monopolar mode does not have such angular phase variation, it is convenient to express the scattered field for the dipolar mode only to understand the emergence of its rotating shape. By substituting expressions of spherical harmonics corresponding to the mode $n = 1$ and by using expression (8), the partial dipolar scattered field is expressed as follows:

$$\phi_{\mathrm{s}}^{\mathrm{dip}}(r,\theta,\varphi) = \left[\frac{s_0^1}{\sqrt{2}}\cos\theta - s_1^1 \sin\theta\cos\varphi\right]\sqrt{\frac{3}{2\pi}}\, h_1^{(1)}(k_0 r). \tag{9}$$

Then, it can be decomposed into two spiral fields (ϕ_+ in $\mathrm{e}^{\mathrm{i}\theta}$ and ϕ_- in $\mathrm{e}^{-\mathrm{i}\theta}$) which have a

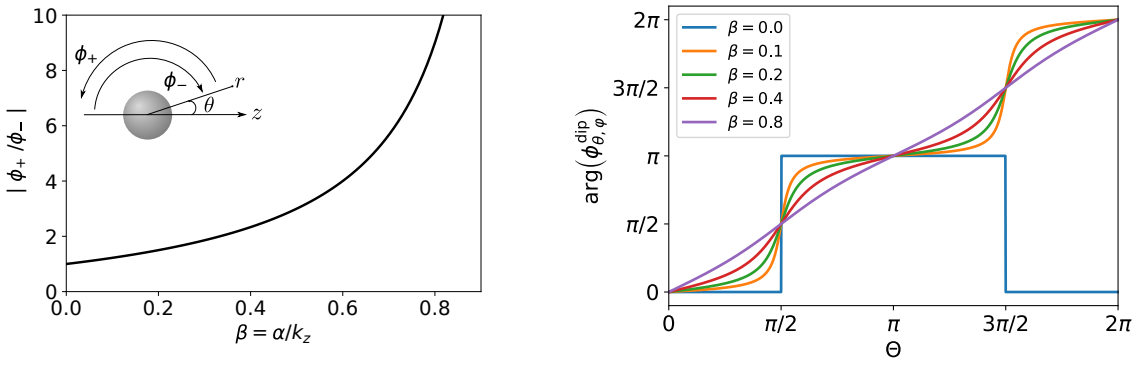

(a) (b)

Figure 6: (a) Ratio $|\phi_+/\phi_-|$ computed for $\varphi = 0$ as a function of β. (b) Phase of the angular part of scattered field $\phi^{\text{dip}}_{\theta,\varphi}$ as a function of the angle $\Theta \in [0, 2\pi]$ in the (xz)-plane.

polar phase variation:

$$\begin{aligned}\phi^{\text{dip}}_{\text{s}}(r,\theta,\varphi) &= \left[\left(\frac{s^1_0}{\sqrt{2}} + \text{i}s^1_1\cos\varphi\right)\text{e}^{\text{i}\theta} + \left(\frac{s^1_0}{\sqrt{2}} - \text{i}s^1_1\cos\varphi\right)\text{e}^{-\text{i}\theta}\right]\sqrt{\frac{3}{8\pi}}h^{(1)}_1(k_0 r)\\ &= \left[\phi_+\text{e}^{\text{i}\theta} + \phi_-\text{e}^{-\text{i}\theta}\right]\sqrt{\frac{3}{8\pi}}h^{(1)}_1(k_0 r)\end{aligned} \tag{10}$$

By separating radial and angular contributions, we can express the angular part of the partial dipolar scattered field as $\phi^{\text{dip}}_{\theta,\varphi} = \phi_+\text{e}^{\text{i}\theta} + \phi_-\text{e}^{-\text{i}\theta}$. We can see that the asymmetry is strongly pronounced for $\varphi = 0$ or π (*i.e.* in the (xz)-plane) and is cancelled in the horizontal (yz)-plane ($\varphi = \frac{\pi}{2}$). By taking the spherical Hankel function asymptotic form for $k_0 r >> 2\pi$, the partial dipolar scattered field is expressed in the far field as:

$$\phi^{\text{dip}}_{\text{s}}(r,\theta,\varphi) = -\sqrt{\frac{3}{8\pi}}\,\phi^{\text{dip}}_{\theta,\varphi}\,\frac{\text{e}^{\text{i}k_0 r}}{k_0 r}. \tag{11}$$

In the case of a homogeneous incident wave, both spiral fields induced by the scattering process are equal in amplitude because the term s^1_1 is null. In the other hand, if the incident wave is evanescent, fields in $\text{e}^{\text{i}\theta}$ and $\text{e}^{-\text{i}\theta}$ have unbalanced amplitudes. This imbalance can be adjusted by increasing β as it is shown in Fig. 6a. The shape of the resulting field is thus drived by the predominant spiral field. By taking $\varphi = 0$, the ϕ_+ field in $\text{e}^{\text{i}\theta}$ is higher in amplitude than the ϕ_- field and thus the phase of the resulting field rotates counterclockwise.

For practical reasons, we introduce a new angle $\Theta \in [0, 2\pi]$ covering the whole (xz)-plane such as $\Theta \in [0, \pi]$ corresponds to $(\theta, \varphi = 0)$, and $\Theta \in [\pi, 2\pi]$ to $(2\pi - \theta, \varphi = \pi)$. The phase evolution of $\phi^{\text{dip}}_{\theta,\varphi}$ as a function of the angle Θ is plotted in Fig. 6b for different values of β. For a homogeneous incident wave, the partial scattered field has a dipolar phase profile as expected for the mode $n = 1$. However, for the evanescent case, the phase of the partial dipolar scattered field is spatially enriched and takes regulary all values in the $[0, 2\pi]$ interval. By increasing β, the latter tends to evolve linearly with Θ. Therefore, for high β, the partial scattered field tends to have an Archimedes' spiral shape in the far field which is caracterized by an equiphase line of the form $r = -A\Theta + B$ where A and B are constants.

3.3. Higher resonances

The spiral structure of the scattered field comes from the generation of spiral waves which appear by increasing the evanescence degree β. The second important parameter is the exciting reduced

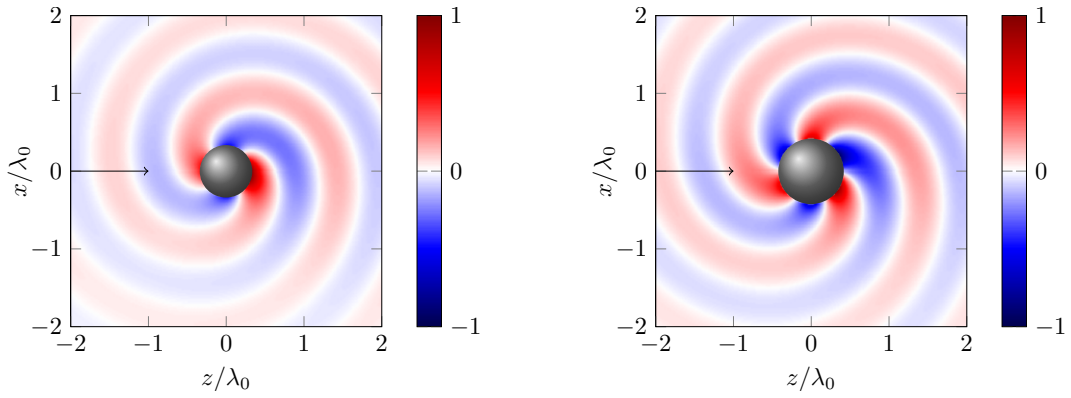

Figure 7: Real part of the scattered acoustic pressure field in the (xz) plane for $\beta = 0.6$ and for higher resonance frequencies of the particle corresponding respectively to the quadrupolar resonance $k_0a = 2$ (a) and the hexapolar resonance $k_0a = 2.53$ (b).

frequency k_0a which sets the contribution of each mode. Effects of higher modes on the spiral are then analysed in this section.

For the same frequency as before, the particle radius is chosen to excite the quadrupolar and hexapolar resonances. The real part of the scattered field is shown in Fig. 7. As for the dipolar resonance, the scattered field has a rotating shape around the scatterer but in this case its phase takes values in the $[0, 2\pi]$ interval respectively two and three times during a period. Technically, the scattered field could also be expressed in terms of spiral waves which have angular variations in $\mathrm{e}^{\pm 2\mathrm{i}\theta}$ for the quadrupolar mode and $\mathrm{e}^{\pm 3\mathrm{i}\theta}$ for the hexapolar mode. Therefore, when a particular mode is preferably excited by choosing the right exciting frequency, the number of 2π-jumps is relative to the characteristic number of this mode. It can be expected that an absorbent particle placed in an evanescent field in a viscous medium would rotate and that the rotation speed would increase with the highest mode numbers, n [17, 18].

4. Conclusion

The scattering of a plane wave by a spherical object gives rise to the generation of spiral waves around the object which do not have the same amplitude for an evanescent excitation. A spiral phase distribution of the scattered field can be obtained in this case and the number of 2π-jumps of the phase depends on the mode which contributes the most in the field. Due to its rotating structure, the scattered field carries an angular momentum which should result in a non-null radiation torque.

Near field applications can be considered such as particle rotation control, or applications that take advantage of the fact that a significant field is radiated in all directions like imaging. Very recently, several works in optics and acoustics deal with the propagation directionality of guided modes using an active circular source [19, 20]. As part of this work, the circular scattered field obtained could serve as a passive source.

Experiments that enable observations of particle rotation in an evanescent field are envisaged. We may also consider radiation forces induced by evanescent fields for particle translations [21]. Field interactions with an interface may also be taken into account in future work.

Appendix A. Scattering and internal field coefficients of a fluid scatterer

In the case of a fluid scatterer, modal coefficients of scattered and internal velocity-potentials are given respectively by:

$$S_n = -\frac{q\, j_n'(k_0a)\, j_n(k_1a) - j_n(k_0a)\, j_n'(k_1a)}{q\, h_n^{(1)\prime}(k_0a)\, j_n(k_1a) - h_n^{(1)}(k_0a)\, j_n'(k_1a)}$$

$$B_n = \frac{-h_n^{(1)}(k_0a)\, j_n'(k_0a) + h_n^{(1)\prime}(k_0a)\, j_n(k_0a)}{-\frac{k_1}{k_0}\, h_n^{(1)}(k_0a)\, j_n'(k_1a) + \frac{\rho_1}{\rho_0}\, h_n^{(1)\prime}(k_0a)\, j_n(k_1a)} \tag{A.1}$$

with $q = \frac{\rho_1\, k_0}{\rho_0\, k_1}$, a the sphere radius, and where $'$ denotes the derivative with respect to the variable k_0a or k_1a.

References

[1] Bazylewski P, Ezugwu S and Fanchini G 2017 A review of three-dimensional scanning near-field optical microscopy (3D-SNOM) and its applications in nanoscale light management *Applied Sciences* **7** 10 973.
[2] Aubert V, Wunenburger R, Valier-Brasier T, Rabaud D, Kleman J P and Poulain C 2016 A simple acoustofluidic chip for microscale manipulation using evanescent Scholte waves *Lab on a Chip* **16** 13 2532-2539.
[3] Osterhoudt C F and Marston P L 2006 Scattering of evanescent waves incident on targets in a simulated sediment *J. Acoust. Soc Am.* **120** 5 3143-3144.
[4] Kawata S and Sugiura T 1992 Movement of micrometer-sized particles in the evanescent field of a laser beam *Optics Letters* **17** 11 772-774.
[5] Bliokh K Y, Bekshaev A Y and Nori F 2014 Extraordinary momentum and spin in evanescent waves *Nature Communications* **5** 1 1-8.
[6] Almaas E and Brevik I 2013 Possible sorting mechanism for microparticles in an evanescent field *Physical Review A* **87** 6 063826.
[7] Baresch D, Thomas J L and Marchiano R 2016 Observation of a single-beam gradient force acoustical trap for elastic particles: acoustical tweezers *Physical Review Letters* **116** 2 024301.
[8] Chew H, Wang D S and Kerker M 1979 Elastic scattering of evanescent electromagnetic waves *Applied Optics* **18** 15 2679-2687.
[9] Quinten M, Pack A and Wannemacher R 1999 Scattering and extinction of evanescent waves by small particles *Applied physics B: Lasers and Optics* **68** 1.
[10] Bekshaev A Y, Bliokh K Y and Nori F 2013 Mie scattering and optical forces from evanescent fields: A complex-angle approach *Optics Express* **21** 6 7082-7095.
[11] Abramowitz M and Stegun I A 1965 Handbook of mathematical functions *Dover Publications.*
[12] Almaas E and Brevik I 1995 Radiation forces on a micrometer-sized sphere in an evanescent field *J. Opt. Soc Am. B* **12** 12 2429-2438.
[13] Jaising H Y and Hellesø O G 2005 Radiation forces on a Mie particle in the evanescent field of an optical waveguide *Optics Communications* **246** 4-6 373-383.
[14] Martin P A 2006 Multiple scattering: interaction of time-harmonic waves with N obstacles *Cambridge University press.*
[15] Brunet T, Zimny K, Mascaro B, Sandre O, Poncelet O, Aristgui C and Mondain-Monval O 2013 Tuning Mie scattering resonances in soft materials with magnetic fields *Physical Review Letters* **111** 26 264301.
[16] Tallon B, Brunet T and Page J H 2017 Impact of strong scattering resonances on ballistic and diffusive wave transport *Physical Review Letters* **119** 16 164301.
[17] Zhang L and Marston P L 2014 Acoustic radiation torque on small objects in viscous fluids and connection with viscous dissipation *J. Acoust. Soc Am.* **136** 6 2917-2921.
[18] Silva G T 2014 Acoustic radiation force and torque on an absorbing compressible particle in an inviscid fluid *J. Acoust. Soc Am.* **136** 5 2405-2413.
[19] Picardi M F, Zayats A V and Rodríguez-Fortuño F J 2018 Janus and Huygens' dipoles: near-field directionality beyond spin-momentum locking *Physical Review Letters* **120** 11 117402.
[20] Long Y *et al.* 2020 Symmetry Selective Directionality in Near-Field Acoustics *National Science Review.*
[21] Baresch D, Thomas J L and Marchiano R 2013 Three-dimensional acoustic radiation force on an arbitrarily located elastic sphere *J. Acoust. Soc Am.* **133** 1 25-36.